Mars *in situ* oxygen and propellant production by non-equilibrium plasmas

P. Ogloblina[1,2], A. S. Morillo-Candas[2], A. F. Silva[3], T. Silva[1], A. Tejero-del-Caz[4], L. L. Alves[1], O. Guaitella[2] and V. Guerra[1]

[1] Instituto de Plasmas e Fusão Nuclear, Instituto Superior Técnico, Universidade de Lisboa, Portugal

[2] Laboratoire de Physique des Plasmas (UMR 7648), CNRS-Univ. Paris Sud-Sorbonne Université-École Polytechnique 91128 Palaiseau, France

[3] Dutch Institute For Fundamental Energy Research (DIFFER), Eindhoven, The Netherlands

[4] Departamento de Física, Universidad de Córdoba, Spain

E-mail: vguerra@tecnico.ulisboa.pt

August 2017

Abstract. It has been recently advocated that Mars has excellent conditions for oxygen and fuel production directly from atmospheric CO_2 using non-equilibrium plasmas. The Martian conditions would be favorable for vibrational excitation and/or enhanced dissociation by electron impact, two important pathways for CO_2 plasma dissociation. Herein we confirm these theoretical predictions by measuring, for the first time, the vibrational temperatures of CO_2 and the CO and CO_2 concentrations in realistic Martian conditions. *In situ* Fourier transform infrared spectroscopy (FTIR) measurements are performed in experiments conducted in DC glow discharges operating at pressures $p = 1 - 5$ Torr, discharge currents $I = 10 - 50$ mA, initial gas temperatures of 220 K and 300 K, both in pure CO_2 and in the synthetic Martian atmosphere 96%CO_2-2%Ar-2%N_2. To analyse and interpret the experimental results, we develop a detailed self-consistent kinetic model for pure CO_2 plasmas, describing the coupled electron and heavy-particle kinetics. The simulation results are in very good agreement with the experimental data. It is shown that the low-temperature conditions may enhance the degree of vibrational non-equilibrium and that the Martian atmospheric composition has a positive effect on CO_2 decomposition. Accordingly, the present investigation confirms the potential of plasma technologies for in-situ resource utilization (ISRU) on Mars.

Keywords: In situ resource utilisation, Mars, oxygen production, plasma, CO2 dissociation

Submitted to: *Plasma Sources Sci. Technol.*

1. Introduction

Mars exploration draws ever more attention nowadays, with new plans from space agencies and private companies announced frequently [1]. Current missions to the surface of the red planet

focus on robotic landers and rovers, but proposals for the first human missions and settlements will certainly follow soon. Future missions will require the ability to collect resources *in situ* and transform them into breathable air, water, propellants or food. Mars has resources that can be used for a sustainable settlement, such as carbon dioxide, which is the most abundant (95.9%) component of its atmosphere, with smaller percentages of Ar (1.9%), N_2 (2.6%) and other gases [2]. The local production of oxygen on Mars directly from atmospheric CO_2 may help solving some of these challenges, such as manufacturing fuels to get back to Earth, and creating a breathable environment for a future outpost.

The idea to try to use CO_2 as a raw material for *in situ resource utilization* (ISRU) on Mars for rocket propellant production dates back to the late 1970s, with the pioneering works of Ash and collaborators [3,4]. CO_2 can be converted into carbon monoxyde (CO) and oxygen (O_2) and used in a CO/O_2 propellant or, with some hydrogen brought from Earth or produced from Martian water, into oxygen and methane, the latter via the Sabatier process $CO_2+4H_2 \rightarrow CH_4+2H_2O$. Several authors have discussed the feasibility of using local resources for fuel or oxygen manufacturing, and the references given here are merely indicative. Landis and Linne [5] proposed the construction of a reusable hopper vehicle that could self-refuel, making its fuel from a zirconia-electrolysis oxygen generation system. Boiron and Cantwell [6] discuss the possibility of hybrid rocket propulsion systems, based on a combination of a liquid oxidizer and a solid fuel, where the oxidizer is acquired through decomposition of carbon dioxide on the surface of Mars. A review of the state-of-the-art on Mars ISRU was published in 2015 by Sanders *et al* [7]. In the last few years, solid oxide electrolysis for fuel and oxygen production from the Martian atmosphere [4] has caught a lot of attention, due to its choice for the thrilling Mars Oxygen ISRU Experiment (MOXIE) instrument on the Mars 2020 mission [8–10], a choice dictated by the simplicity and robustness of this already existing technology.

Gaseous CO_2 can be converted into O_2 and CO using different methods, that are the subject of a large scientific activity for applications on Earth. As a matter of fact, due to the continuous growth of fossil fuel consumption and the steady increase of anthropogenic greenhouse gas emissions [11], the scientific community is actively investigating how to replace fossil fuels by solar fuels, *i.e.*, how to produce synthetic fuels from renewable electricity, using CO_2 as a raw material. The bottleneck in this scheme is achieving an efficient CO_2 dissociation, in a process compatible with the geographic constraints and intermittency of renewable energy sources. Low-temperature plasmas provide a very interesting context to address the problem [12]. In this rich medium, several dissociation pathways are possible: the high-energy electrons can directly dissociate the CO_2 molecule; high-power plasma sources may significantly heat the gas and enhance thermal dissociation; and in typical conditions found for operation of various discharges the electrons can efficiently transfer their energy into the vibrational excitation of CO_2, that can be subsequently up-pumped along the asymmetric stretching mode to high levels and enhance dissociation via non-equilibrium processes [12,13]. The latter process is essential to achieve high energy efficiencies for CO_2 conversion, above those obtainable under thermally-driven processes. There are many other advantages of plasma technologies besides energy efficiency, such as the possibility of instant start and stop of operation, scalability, and its relatively cheap design that does not require the use of scarce

materials.

Even though CO_2 reforming is a widely discussed topic and a vast research is devoted to it in terms of reduction of greenhouse emission, production of solar fuels and chemical materials on Earth, very few studies are available regarding the use of plasmas in Martian conditions. The suggestion to use plasmas for ISRU on Mars dates back to the 1990s in a series of papers by Outlaw and co-workers [14–16], with a very recent follow-up by Premathilake *et al* [17]. Alternative ideas have been proposed by Gruenwald [18]. Some works related to plasmas on Mars do not focus on ISRU and address, *e.g.*, the characterisation of electrical discharges in CO_2/Ar/N_2 mixtures [19, 20], the study of vibrational-energy transfers in spacecraft entry conditions [21], or the calculation of cross sections [22] and transport coefficients [23] for the dominant heavy-particles in the Martian atmosphere.

In a recent study, we have put forward a strong case for oxygen and propellant production on Mars directly from the atmosphere using low-temperature plasmas, by showing that Mars has nearly ideal conditions for CO_2 dissociation by plasmas [24, 25]. In particular, it was advocated that: i) the pressure on the surface of Mars ($\sim$ 4.5 Torr) is very suitable for plasma operation, since the discharge tends to be homogeneous and is easy to ignite; ii) the cold Martian atmosphere may enhance vibration-vibration (V-V) up-pumping and hinder vibration-translation (V-T) deactivation, favoring dissociation via the indirect route that takes advantage of vibrational non-equilibrium; iii) Ar and N_2 may shift the electron energy to higher values and help pumping the CO_2 asymmetric stretching mode, respectively, contributing as well to enhance dissociation and increase its efficiency. The simulations in [24, 25] show very promising results, but no experimental confirmation of these predictions was attempted to date.

Herein we undertake a joint experimental and modeling investigation to assess the validity of the ideas advanced in [24, 25]. To this purpose, experiments are carried out in plasmas created in simple and reproducible DC glow discharges, in pure CO_2 and in a synthetic Martian atmosphere of 96% of CO_2 with 2% of Ar and 2% of N_2, for pressures in the range 0.5-6 Torr, discharge currents from 20 to 50 mA, both with the input gas at room temperature (300 K) and typical Mars average temperatures (220 K). The CO_2 and CO vibrational temperatures, the conversion factor, and the gas temperature are measured in these conditions using *in situ* Fourier transform infrared (FTIR) spectroscopy, while the reduced electric field is determined from the voltage drop between two tungsten probes at the floating potential. The bases of the experimental set-up are similar to the ones used in former fundamental studies on CO_2 reforming on Earth [26, 27]. The low-temperature Martian conditions are recreated here by immersing the plasma reactor in a bath of dry ice and ethanol. To the best of our knowledge, these measurements constitute the first experimental characterization of plasmas created in a realistic Martian environment and address, at the same time, the vibrational non-equilibrium and the CO_2 conversion in these plasmas. Preliminary results were presented in [28].

To complement the experimental study, a detailed self-consistent kinetic model is developed to analyze and interpret the experimental data obtained in pure CO_2. The model describes the electron kinetics, by solving the electron Boltzmann equation for a CO_2/CO/O_2/O mixture [29, 30] using the two-term Boltzmann solver LoKI-B [31], coupled with the heavy-

particle kinetics, described by a set of rate balance equations for the creation and destruction of the most important neutral and charged heavy-particles in the plasma, namely $CO_2(\nu_1\nu_2^{l_2}\nu_3)$, $CO(X\ ^1\Sigma^+, a\ ^3\Pi_r)$, $O_2(X\ ^3\Sigma_g^-, a\ ^1\Delta_g, b\ ^1\Sigma_g^+)$, $O(^3P, ^1D)$, O_3, CO_2^+, CO^+, O_2^+, O^+, and O^-, following the formulation from [32] and implemented in the LoKI simulation tool as described in [33, 34]. Here, $CO_2(\nu_1\nu_2^{l_2}\nu_3)$ accounts for 72 individual CO_2 vibrational levels (see section 3). This model constitutes a major improvement regarding our previous simulations for CO_2 plasmas, where only the coupling between the electron kinetics and the $CO_2(\nu_1\nu_2^{l_2}\nu_3)$ vibrational levels is taken into account [35–38], or where no vibrational excited states of CO_2 are considered [39], or where vibrational states of CO_2 are included with very reduced set of chemical reactions [40]. In addition, vibrational relaxation of $CO_2(\nu_1\nu_2^{l_2}\nu_3)$ molecules in collisions with O atoms is now included as in [41] and is shown to have a significant influence in shaping the CO_2 vibrational distribution functions. Vibrational relaxation in CO_2-O_2 collisions is also accounted for.

The structure of this paper is as follows. Section 2 briefly describes the experimental setup and the diagnostics used. Section 3 details the formulation of the model and describes the input data. The experimental and modelling results are presented and discussed in section 4. Finally, section 5 summarises our main findings.

2. Experiment

The experimental setup and diagnostics used are very similar to those described in [26,27]. In addition, a new system had to be devised and included in the setup to reproduce the Martian low-temperature conditions, as further described below.

The plasma reactor under study is a cylindrical-shaped Pyrex tube, with a 2 cm inner diameter and a length of 23 cm. The electrodes are positioned 17 cm apart, opposite to the gas in- and outlet. The reactor is connected in series with a 40 kΩ resistor to a DC power supply. The electric field in the reactor is measured with two tungsten pins radially pointing inside the positive column of the glow discharge. The positive column can be considered homogeneous [42] and, therefore, the measurement of the electric field with two pins gives the value of the average field in the whole bulk of the plasma. The discharge current is varied between 10 and 50 mA. The pressure is varied between 0.5 and 5 Torr, using a scroll pump (Edwards XDS-5), and a pressure gauge (Pfeiffer CMR263) with feedback to an automated pressure regulating valve (Pfeiffer EVR116) and controller (Pfeiffer RVC300).

The experiments are conduced both in pure CO_2 and in a synthetic Martian atmosphere corresponding to a mixture of 96% CO_2 with 2% of Ar and 2% of N_2 (all Air Liquide Alphagaz 1). The gas flows are controlled using mass flow controllers (Bronkhorst F-201CV). A total gas flow of 7.4 sccm has been used in our previous work comparing experiment with models [35, 37, 39, 41] and is employed as well as the reference condition in the present experiments. However, to insure a good precision of the concentration of the small admixtures of Ar and N_2 necessary to reproduce the Martian mixture, for the corresponding additional measurements a larger total gas flow of 19.25 sccm is used, composed of 0.39 sccm of nitrogen and 0.39 sccm of argon and the remainder of CO_2.

The reactor is positioned in the sample compartment of a FTIR spectrometer (Bruker V70) as presented in figure 1. The chosen configuration ensures that the IR absorption measurements (line-of sight-integrated) are taken only through the positive column of the glow discharge. The contribution of the IR emission from the plasma is subtracted to the transmission spectra. The detected IR spectra contain several lines of CO and CO_2 vibrational transitions and are fitted according to the procedure described by Klarenaar *et al* [26, 43]. It is assumed that the rotational and vibrational temperatures are uniform along the length of the positive column. As an outcome of the fitting procedure, the vibrational temperatures of CO_2 and CO, the rotational temperature of CO and CO_2 - assumed to be representative of the gas temperature [27] - , and the dissociation fraction

$$\alpha = \frac{[CO]}{[CO] + [CO_2]} ,$$

where [CO] and [CO_2] represent the gas phase concentrations of CO and CO_2 molecules, respectively, are obtained from the acquired spectra.

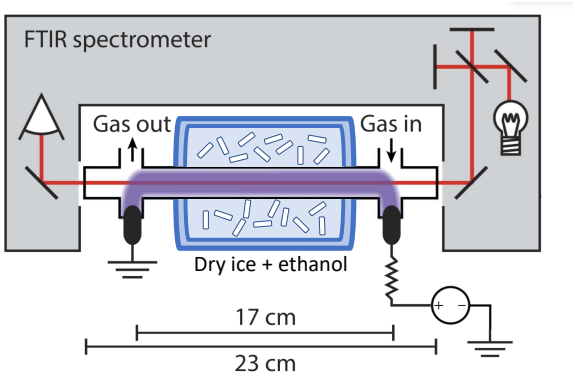

Figure 1. Schematic representation of the discharge reactor placed in the sample compartment of the FTIR spectrometer and immersed in a mixture of dry ice and ethanol. Adapted from [26].

To mimic Mars-like temperature conditions, the reactor is immersed into a mixture of dry ice and ethanol, as shown in the photos of the setup and the discharge in figure 2. Both the mixture temperature and the gas temperature inside the reactor before igniting the plasma are controlled with a temperature dependent platinum thin film chip resistor (Vishay PTS 0603). The nominal resistance temperature specifications from the manufacturer (given down to 215 K) was cross checked by calibrating it with a chiller (Huber 230) down to 243 K. The temperature of the gas before experiencing the plasma is further controlled by the FTIR measurements and is approximately 220–230 K. Both techniques agree within a 5% error for "plasma off" gas temperature measurements. As the temperature probe sensor is a an intrusive diagnostics, it is not used for the "plasma on" measurements and only the results obtained from the FTIR absorption spectra are considered. For the Earth temperature conditions, the same operating conditions were tested without surrounding the reactor by the dry ice and ethanol bath.

Figure 2. Discharge reactor immersed into a mixture of dry ice and ethanol and positioned in the sample compartment of the FTIR when the plasma is ON.

3. Model

A self-consistent kinetic model was developed to interpret the experimental results and describe the detailed kinetics of the major species in plasmas created in DC CO_2 discharges. It couples the electron, vibrational, chemical and ion kinetics, and builds on previous models for CO_2-containing plasmas, already tested and validated in discharges and afterglows and for various operating conditions [35–39, 41]. The model takes as input the parameters controlled in a real experiment, in particular the discharge current, I, pressure, p, gas flow, Φ, and tube radius, R. Additionally, in the present simulations the gas temperature, T_g, is also given as an input parameter, since its value is available from experiment and our purpose is not to focus on the gas heating mechanisms but rather on the plasma chemistry in the system. Note that the gas thermal balance equation can be incorporated in the present formulation, as it was already done in [38].

The EEDF is obtained from the solution of the homogeneous and stationary electron Boltzmann equation in a $CO_2/CO/O_2/O$ mixture, solved in the usual two-term expansion in Legendre polynomials. The calculations are done with the LisbOn KInetics Boltzmann solver LoKI-B [33, 34], an in-house code developed in object-oriented programming under MATLAB® and distributed in open source. The electron impact cross sections for the different gases have been previously validated and are described in [29] for CO_2, [30] for

CO, and in [44] for O_2 and O, and can be obtained from IST-Lisbon database at the open-access web-platform LXCat [45]. These cross sections have been mostly based on [46–48] for CO_2, [49–54] for CO, [55, 56] for O_2 and [57] for O. The EEDF is calculated taken into account elastic and inelastic collisions of electrons with the parent gases, whose concentrations are self-consistently calculated (see below), as well as stepwise and superelastic collisions with vibrationally excited CO_2 and CO molecules and electronically excited metastables molecules $O_2(a, b)$ and $CO(a)$ and atoms $O(^1D)$.

The electron Boltzmann equation is coupled to a system of rate balance equations describing the creation and loss of neutral and charged heavy-species, using the approach from [32, 58]. The resulting global model is simulated with the LoKI simulation tool [33, 34]. The species considered in the model include: 72 vibrationally excited CO_2 levels, represented as $CO_2(\nu_1\nu_2^{l_2}\nu_3)$, where $\nu_1 \leq 2$, $\nu_2 \leq 5$ and $\nu_3 \leq 5$ denote the vibrational quanta in the symmetric stretching, bending, and asymmetric stretching vibrational modes, respectively, and l_2 defines the projection of the angular momentum of bending vibrations onto the axis of the molecule [35]; ground-state and electronically excited CO and O_2 molecules, $CO(X\ ^1\Sigma^+, a\ ^3\Pi_r)$, $O_2(X\ ^3\Sigma_g^-, a\ ^1\Delta_g, b\ ^1\Sigma_g^+)$; ground-state and electronically excited oxygen atoms, $O(^3P, ^1D)$; ground-state and vibrationally excited ozone, O_3 and $O_3^\star$, respectively; and positive and negative ions, CO_2^+, CO^+, O_2^+, O^+, and O^-. Following the results in [40], electron impact dissociation from ground-state $CO_2(00^00)$ molecules is taken into account using the dissociation cross section from Polak and Slovetsky [59]. As discussed in [29], this cross section is not part of the complete and consistent CO_2 cross section set and, accordingly, is not used to obtain the EEDF, but is integrated with the calculated EEDF to obtain the corresponding rate coefficient. Due to the lack of data, the dissociation cross section from vibrationally excited states is considered with a threshold reduction, while keeping the same shape and magnitude as for dissociation from the ground-state. The same threshold reduction procedure is used to account for ionization from vibrationally excited CO_2 molecules. The loss probability of O atoms at the wall, γ_O, is considered with the expression proposed in [27], deduced from the experimental determination of O-atom loss frequencies. The details on the complex plasma chemistry taken into account can be found in previous publications dealing with the CO_2 vibrational kinetics [35, 36], the kinetic mechanisms in O_2 plasmas [60], and the plasma chemistry in vibrationally cold CO_2 [39].

Note that no chemistry was included in [35, 36], a reduced chemistry set with only five reactions was coupled with the vibrational kinetics in [40], while no vibrational kinetics was considered in [39]. Accordingly, the current model constitutes a significant upgrade of our prior models, by describing self-consistently and in detail the coupled electron, vibrational and chemical kinetics. Moreover, in [35, 36] only vibrational energy transfers in CO_2-CO_2 collisions and vibrational deactivation at the wall are considered, as those works focus in the so-called 'single-pulse' experiment, where CO_2 dissociation is very low. However, in a steady-state situation, significant amounts of CO, O_2 and O are present in the plasma (*cf.* section 4). Therefore, we have additionally included vibrational-to-translation (VT) energy exchanges in CO_2-O collisions:

$$CO_2(00^0\nu_3) + O \rightleftharpoons CO_2(02^2(\nu_3 - 1)) + O$$

$$CO_2(00^0\nu_3) + O \rightleftharpoons CO_2(03^3(\nu_3 - 1)) + O$$
$$CO_2(00^0\nu_3) + O \rightleftharpoons CO_2(04^4(\nu_3 - 1)) + O$$
$$CO_2(0\nu_2^{\nu_2}0) + O \rightleftharpoons CO_2(0(\nu_2 - 1)^{\nu_2-1}0) + O\,,$$

as they can affect significantly the vibrational distribution functions even for relatively small amounts of atomic oxygen [41, 61]. The corresponding rate coefficients are given in [62] for $\nu_2 = 1$ and $\nu_3 = 1$ and the harmonic oscillator scaling (linear with ν_2 or ν_3) is assumed for $\nu_2, \nu_3 > 1$. CO_2-O_2 VT processes are further included, also according to [62]. However, for the present conditions their influence is much smaller than the quenching by atomic oxygen.

Some of the most important reactions considered in the model are listed in Table 1 alongside with corresponding references. This is by no means an exhaustive list and its main purpose is to guide the discussion in section 4. The reader should refer to our publications [35, 36, 39, 60] for a complete kinetic scheme. The rate coefficients for the heavy-particle reactions involving the metastable state $CO(a\ ^3\Pi_r)$ are discussed in [39]. The rate coefficient for CO_2 dissociation in collisions involving vibrationally excited $CO_2(\nu_1\nu_2^{l_2}\nu_3)$ and $CO(a)$, reaction R3c, is considered with the same rate coefficient as for ground-state CO_2, reaction R3b.

The self-consistent sustaining reduced electric field, E/N, is obtained as an eigenvalue to the problem, from the requirement that, under steady-state conditions, the total rate of production of electrons in ionization events must compensate exactly their total loss rate due to ambipolar diffusion and electron-ion recombination, while respecting quasi-neutrality [32,58]. A generic flowchart of the algorithm used to couple the electron, neutral, and ion kinetics, is presented in [64] and an updated scheme is available at the LoKI website [34].

4. Results and Discussion

This section presents and analyses the experimental and simulation results in continuous DC discharges at pressures $p = 0.5 - 5$ Torr, discharge currents $I = \{20, 50\}$ mA, addressing: *i)* the differences induced by Earth and Mars atmospheric temperature conditions in the plasma chemistry in pure CO_2 (section 4.1); *ii)* the influence of the ambient temperature on the vibrational kinetics of CO_2 (section 4.2); *iii)* the effect of the Mars atmospheric minor constituents N_2 and Ar in CO_2 decomposition (section 4.3). The total gas flow is $\Phi = 7.4$ sccm for i) and ii) and $\Phi = 19.25$ sccm for iii).

4.1. CO_2 plasma chemistry at Mars and Earth temperature conditions

We first investigate the influence of the ambient temperature on the plasma chemistry in pure CO_2 plasmas, while keeping the pressure around the Martian atmospheric pressure. For this purpose, we compare the results obtained when the plasma is ignited at Martian (~ 220 K) or Terrestrial (~ 300 K) ambient temperatures, in order to find out up to which extent the results obtained on Earth at low pressure can be assumed to be valid on Mars.

Figure 3 shows the measured and calculated values of the reduced electric field, E/N, as a function of the gas density (N) $\times$ tube radius (R) product for currents $I = 20$ mA and

Table 1. List of some important reactions mentioned in the text.

R1a	$CO(a) + O_2(X) \rightarrow CO(X) + O(^3P) + O(^3P)$	[39]
R1b	$CO(a) + O_2(X) \rightarrow CO(X) + O_2(X)$	[39]
R2	$CO(a) + CO(X) \rightarrow CO(X) + CO(X)$	[39]
R3a	$CO(a) + CO_2 \rightarrow CO(X) + CO_2$	[39]
R3b	$CO(a) + CO_2(00^00) \rightarrow CO(X) + CO(X) + O(^3P)$	[39]
R3c	$CO(a) + CO_2(\nu_1 \nu_2^{l_2} \nu_3) \rightarrow CO(X) + CO(X) + O(^3P)$	see text
R4	$CO(a) + O(^3P) \rightarrow CO(X) + O(^3P)$	[63]
R5	$e + CO_2(00^00) \rightarrow e + CO(X) + O(^1D)$	[29]
R6a	$e + CO_2(01^10) \rightarrow e + CO(X) + O(^1D)$	[29]
R6b	$e + CO_2(02^20) \rightarrow e + CO(X) + O(^1D)$	[29]
R6c	$e + CO_2(10^00 + 02^00) \rightarrow e + CO(X) + O(^1D)$	[29]
R7	$O^- + CO(X) \rightarrow e + CO_2(00^00)$	[39]
R8	$e + CO(X) \rightleftharpoons e + CO(a)$	[30]
R9	$CO(a) + O_2(X) \rightarrow CO_2(00^00) + O(^3P)$	[39]
R10	$e + CO_2(00^00) \rightarrow CO(X) + O^-$	[29]
R11	$O_2(b) + O(^3P) \rightarrow O_2(X) + O(^3P)$	[60]
R12	$O_2(a) + \text{wall} \rightarrow O_2(X)$	[60]
R13	$O_2(b) + \text{wall} \rightarrow O_2(X)$	[60]
R14	$O(^3P) + \text{wall} \rightarrow 0.5O_2(X)$	[27]
R15	$e + O_2(X) \rightleftharpoons e + O_2(a)$	[60]
R16	$e + O_2(X) \rightleftharpoons e + O_2(b)$	[60]
R17	$e + O_2(X) \rightarrow e + O(^3P) + O(^3P)$	[60]
R18	$e + O_2(X) \rightarrow e + O(^3P) + O(^1D)$	[60]
R19	$O(^1D) + O_2(X) \rightarrow O(^3P) + O_2(b)$	[60]

50 mA. The E/N values are deduced from two independent measurements: on the one hand, from the electric field evaluation performed by measuring the floating potential of two tungsten pins inserted in the positive column; and, on the other hand, from the measurement of the gas temperature from which the gas density is deduced via the ideal gas law (*cf.* section 2). A true statistical study of reproducibility on these two measurements was not carried out and the error bars shown are only an upper value estimate based on the cumulative errors of these two measurements. The corresponding values of the gas temperature, T_g, obtained from the FTIR measurements of the rotational distribution of CO_2 and CO, are given in Table 2. The gas heating induced by plasma remains very similar for both Mars and Earth conditions and, therefore, the gas temperature for all conditions is essentially shifted from Mars to Earth by an offset typically around 70-80 K. Three notes are worth making. First, there is an excellent agreement between measurements and simulations in Earth conditions. Second, the experimental results show that an increase in the discharge current induces a small raise in the value of E/N. This behavior is well captured in the simulations and is partially due to the easier ionization of CO_2 as compared with CO [30] and to the increase of the dissociation of

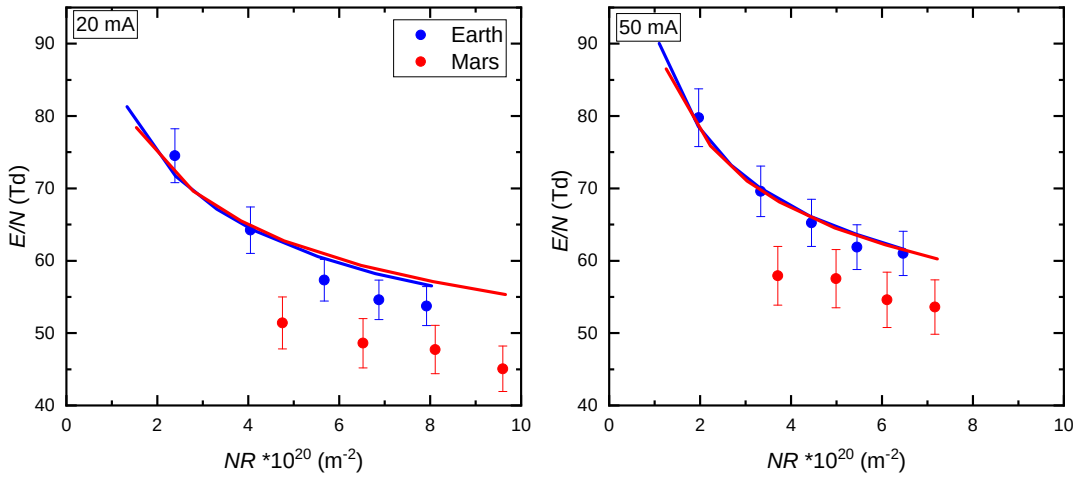

Figure 3. Reduced electric field, E/N, as a function of the NR product, when a pure CO_2 discharge is ignited at Mars and Earth background temperatures at currents $I = 20$ mA (left panel) and $I = 50$ mA (right panel): experiment (•), self-consistent calculation (—).

Table 2. Measured gas temperature (K) deduced from rotational temperature of CO and CO_2 in pure CO_2 plasmas

	20 mA		50 mA	
p (Torr)	Mars	Earth	Mars	Earth
0.5	309	390	380	430
1	348	405	425	490
1.5	378	463	485	555
2	406	477	520	580
3	444	511	580	651
4	476	562	632	709
5	503	610	674	747

CO_2 with the discharge current (see Figure 4), as discussed in [39]. Finally, the measurements further show that the Martian conditions lead to slightly lower values of the reduced electric field than on Earth, although no noticeable variation is found in the self-consistent calculations. These small differences in magnitude between model predictions and measurements in Martian conditions suggest that some details of the charged particle kinetics may be missing in the model, such as temperature dependencies of some rate coefficients, or that improved charged-particle transport data are needed. Overall, the self-consistent calculations of the reduced electric field are in very satisfactory agreement with experiment and the results show that the model can be used as a predictive tool when no experimental data for E/N are available. Here, to avoid an error propagation in the analysis, the experimental values of E/N are given as input to the simulations shown in the remainder of the paper.

The measured and calculated CO_2 dissociation fractions, $\alpha = [CO]/([CO] + [CO_2])$, are

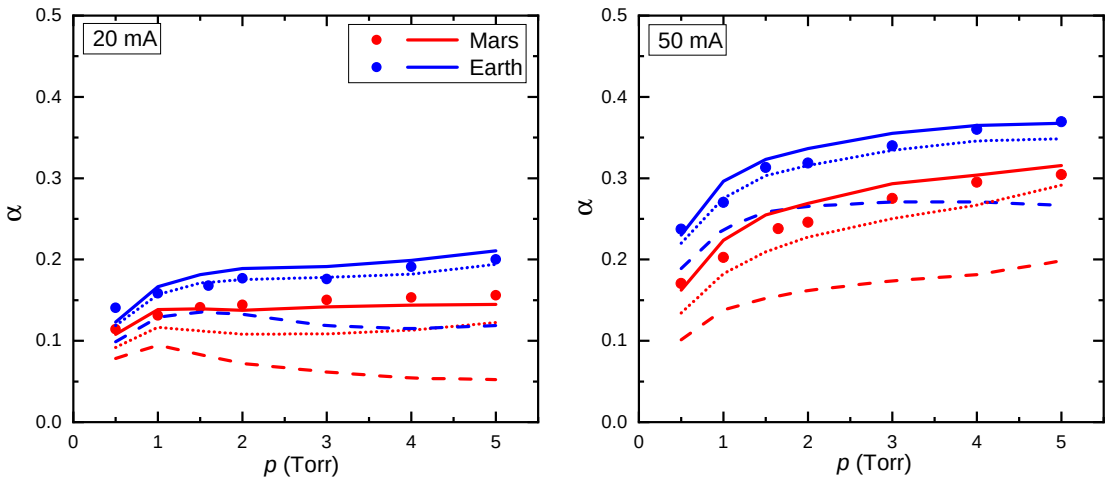

Figure 4. CO_2 dissociation fraction when a pure CO_2 discharge is ignited at Mars and Earth background temperatures at currents $I = 20$ mA (left panel) and $I = 50$ mA (right panel): experiment (•), model calculations by including (—) and excluding (– –) the vibrational kinetics, and by considering the influence of vibrational excited states only in the electron Boltzmann equation (···).

represented in Figure 4. To assess the role of the vibrationally excited states, the calculations are performed both considering (full curves) and neglecting (dashed curves) the vibrational kinetics in the model. Additional simulations are carried out to evaluate the importance of superelastic collisions with vibrationally excited states in shaping the EEDF, by giving the experimental populations of vibrationally excited CO and CO_2 molecules as input to the electron Boltzmann solver, while no vibrationally excited states are considered in the system of rate balance equations for the heavy-particles (dotted curves). There is a quite good agreement between the model predictions and the experimental data. The inclusion of the vibrational kinetics increases the calculated dissociation fraction, as a result of two effects: the modifications of the EEDF due to superelastic collisions with vibrationally excited CO and CO_2, which enhance the high energy-tail [30, 65], and correspond to the differences between the dashed and dotted curves; the contribution of the vibrational states of CO_2 to dissociation by electron impact, reactions (R6), since the rate coefficients for electron-impact dissociation from the vibrationally excited states are higher than from the ground states, corresponding to the differences between the dotted and full curves. Note that the fractional population of the $CO_2(00^00)$ level can be as low as 0.45 (see below), and the corresponding dissociation rate coefficient can be up to 1.7 and 5.6 times smaller than from the (01^10) and the (02^20) levels, respectively. Superelastic collisions have a prominent role in all conditions. In turn, the influence of dissociation from vibrationally excited CO_2 is quite significant on Martian conditions and is relatively small on Earth, due to the lower values of E/N in the former case. Dissociation fractions in the range 10-30% are observed for Martian temperature conditions, which is a promising result regarding the use of plasma technologies for ISRU on Mars, specially taking into account that the present reactor was designed for fundamental studies

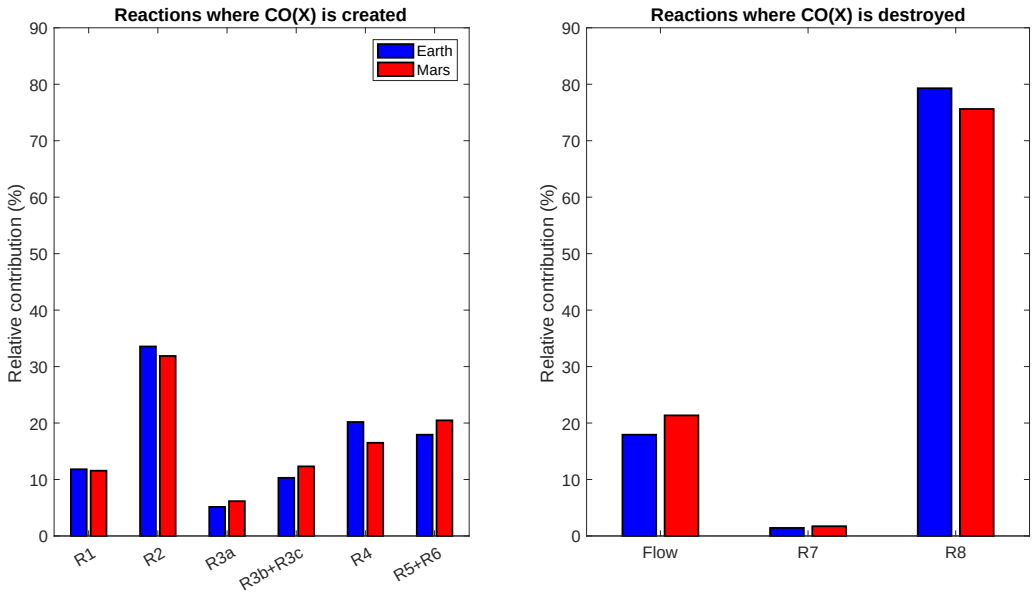

Figure 5. Relative contribution (in %) of the main mechanisms of creation and destruction of CO($X\ ^1\Sigma^+$) when a pure CO_2 discharge at $p = 5$ Torr and $I = 50$ mA is ignited at Mars and Earth background temperatures. The reactions are identified in Table 1.

and is far from any plasma system to be be used in a prototype.

Figure 5 quantifies the contribution of the different creation and destruction mechanisms of CO($X\ ^1\Sigma^+$) molecules for $p = 5$ Torr and $I = 50$ mA. Reactions R1 and R6 in the figure correspond to the total contributions identified in Table 1, R1 = R1a+R1b, R6 = R6a+R6b+R6c. In these conditions, the relative populations of levels (00^00), (01^10), (02^20) and ($10^00 + 02^00$) are 0.453, 0.254, 0.071 and 0.072, respectively. Overall, the dominant mechanisms on Mars and Earth conditions are quite similar. According to the simulations, ground-state CO($X\ ^1\Sigma^+$) molecules are essentially created by dissociation by electron impact on $CO_2(v_1 v_2^{l_2} v_3)$ molecules, mainly on the (00^00), (01^10), (02^20) and the Fermi ($10^00 + 02^00$) states (reactions R5 and R6 in Table 1), and by the quenching of the CO($a\ ^3\Pi_r$) state. The latter mechanism has to be looked at with caution, as the excitation of CO($a\ ^3\Pi_r$) from ground-state CO($X\ ^1\Sigma^+$) is also one of the main processes of destruction of CO($X\ ^1\Sigma^+$), so that reactions involving only CO(X) and CO(a) do not constitute true creation/destruction mechanisms of CO molecules, but rather redistribute its population between the two electronic levels. Nevertheless, processes R3b and R3c do constitue effective creation mechanisms of CO molecules from dissociation of CO_2 in collisions with CO($a\ ^3\Pi_r$) and have a significant contribution to the production of CO. Additional destruction mechanisms of CO($X\ ^1\Sigma^+$) worth mentioning are the transport by the gas flow and the electron-ion recombination reaction R7.

Figures 6-8 show, respectively, the calculated concentrations of the dominant neutral species, electronically-excited states and O_3, and the charged particles. The densities represented in Figure 6 are the total densities of the parent species, *i.e.*, the sum of the populations of all the electronically metastable states; note that for CO_2, CO and O, more than 99.9% of the total population is in the ground electronic state, while for O_2 up to $\sim 20\%$

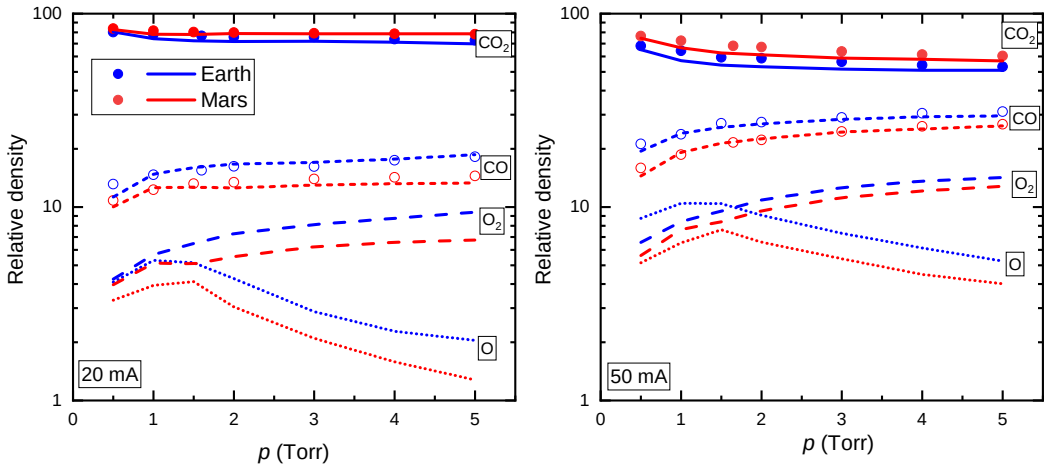

Figure 6. Relative density of the dominant species when a pure CO_2 discharge is ignited at Mars and Earth background temperatures at currents $I = 20$ mA (left panel) and $I = 50$ mA (right panel). The symbols correspond to experimental data for CO_2 (•) and CO (∘).

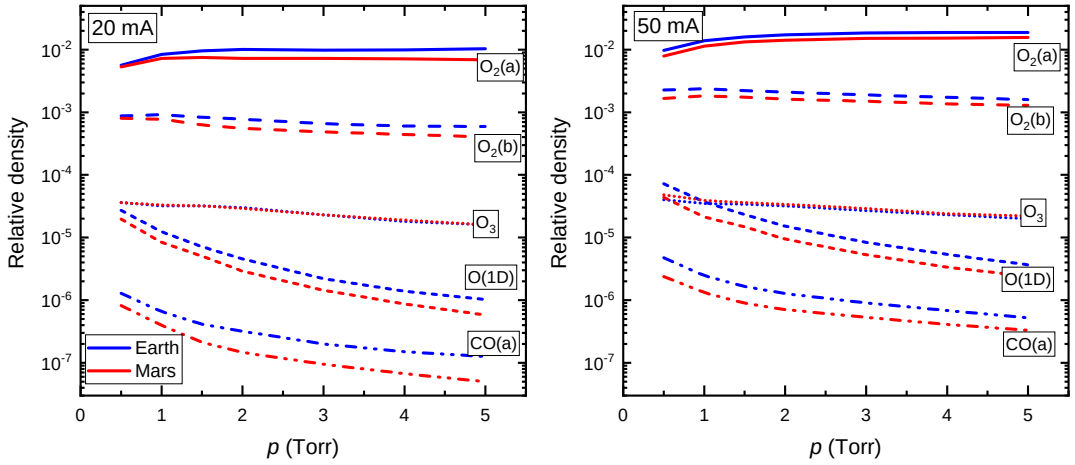

Figure 7. Relative density of various electronically excited states and of ozone, when a pure CO_2 discharge is ignited at Mars and Earth background temperatures at currents $I = 20$ mA (left panel) and $I = 50$ mA (right panel).

of the population can be in the $O_2(a\,^1\Delta_g, b\,^1\Sigma_g^+)$ excited states. Experimental data for CO_2 and CO are also plotted in Figure 6.

Most species represented in Figures 6-8 follow the trend expected by a production dictated by electron-impact dominant mechanisms [39], with a decrease with pressure and an increase with current, as an outcome of the lower reduced electric field (and corresponding lower electron impact rate coefficients) and higher electron density, respectively. A noticeable and important exception to this trend is CO, whose relative concentration remains nearly constant for pressures above $\sim$ 1.5 Torr, although it is mainly produced by electron impact. The increasing behavior of O_2 is partially due to the shift from O to O_2 as the pressure increases and

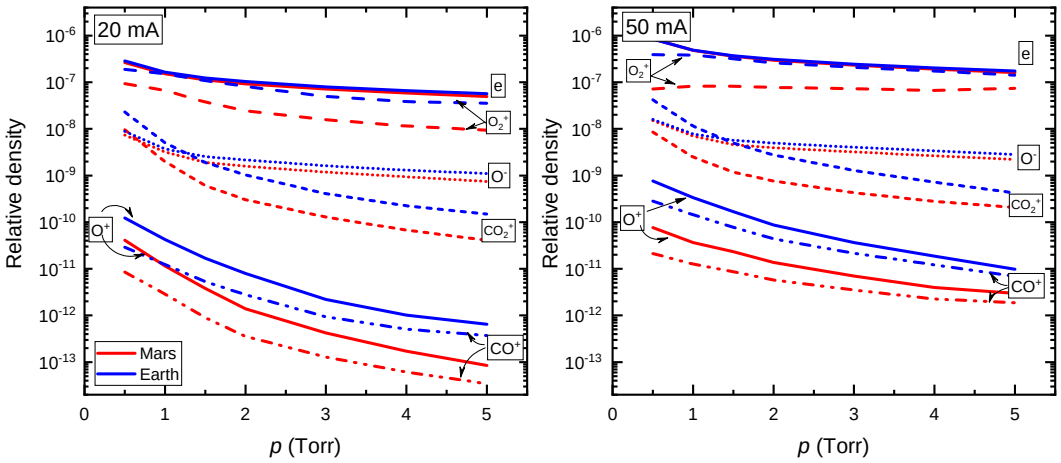

Figure 8. Relative density of various charged particles, when a pure CO_2 discharge is ignited at Mars and Earth background temperatures at currents $I = 20$ mA (left panel) and $I = 50$ mA (right panel).

the associated reduction in the total number of particles. The shift in the relative concentrations of O and O_2 with pressure is mainly a consequence of the increase of the recombination probability of O atoms at the wall with pressure [27], as surface recombination is the main destruction mechanism of O atoms for the present conditions. The O atom densities for the Earth input gas temperature are in a good agreement with the values obtained in [27]. It is also worth noting that O_2^+ is always the dominant ionic species, due to the efficient charge transfer processes from CO_2^+ and O^+ to O_2^+, namely,

$$CO_2^+ + O \rightarrow CO + O_2^+ ,$$
$$O^+ + CO_2 \rightarrow CO + O_2^+ ,$$
$$CO_2^+ + O_2 \rightarrow CO_2 + O_2^+ .$$

Further insight into the complex coupled kinetics taking place in the plasma is given by inspection of figures 9 and 10. Figure 9 displays the relative contribution of the dominant creation and destruction mechanisms of O_2, for the same conditions as in Figure 5, $p = 5$ Torr and $I = 50$ mA. Most of the mechanisms include the excitation from $O_2(X\ ^3\Sigma_g^-)$ to $O_2(a\ ^1\Delta_g)$ or $O_2(b\ ^1\Sigma_g^+)$, or the de-excitation from these excited metastable states back to ground-state. Therefore, they essentially redistribute the population among the three O_2 electronic states. Exceptions are the mechanisms of wall recombination of O atoms (R14), dissociation of O_2 (R17,R18) and dissociation due to the quenching of $CO(a\ ^3\Pi_r)$ (R1a), which, therefore, play a significant role in the kinetics.

Figure 10 depicts the relative contribution of the dominant destruction mechanisms of the $CO(a\ ^3\Pi_r)$ electronically excited state. $CO(a\ ^3\Pi_r)$ is predominantly quenched to $CO(X\ ^1\Sigma^+)$ in collisions with O_2, CO, CO_2 and O, in mechanisms that do not lead to a destruction of a CO molecule. Similarly, it is created by direct electron impact on $CO(X\ ^1\Sigma^+)$ (R8). An effective destruction mechanism of CO molecules is reaction (R9), a back reaction mechanism involving $CO(a\ ^3\Pi_r)$ and O_2 giving back CO_2, recently evinced by Morillo-Candas [66, 67].

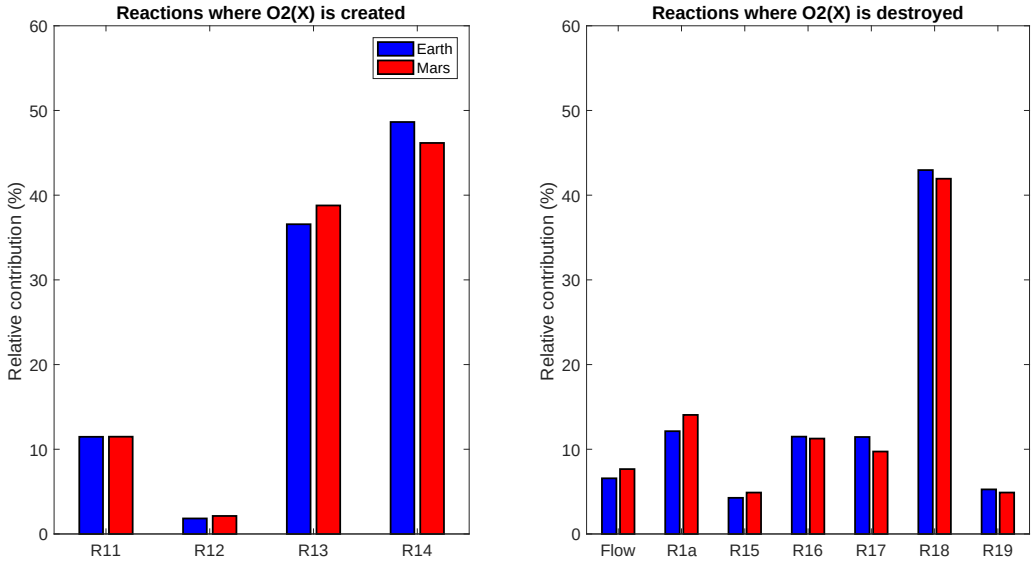

Figure 9. Relative contribution (in %) of the main mechanisms of creation and destruction of $O_2(X\ ^3\Sigma_g^-)$ when a pure CO_2 discharge is ignited at $p = 5$ Torr and $I = 50$ mA at Mars and Earth background temperatures. The reactions are identified in Table 1.

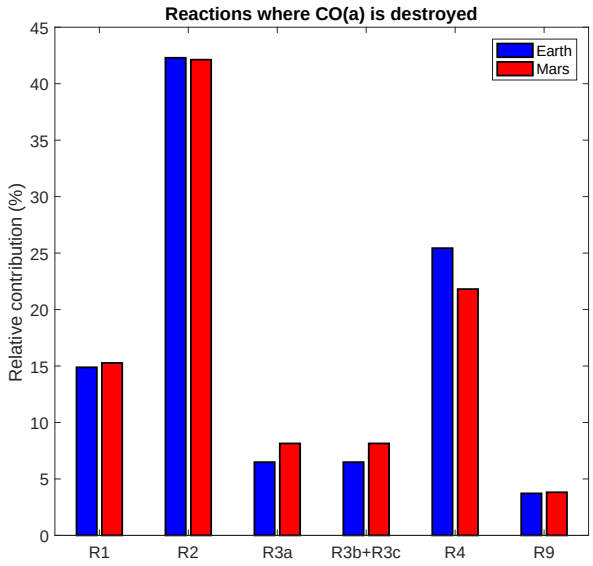

Figure 10. Relative contribution (in %) of the main mechanisms of destruction of $CO(a\ ^3\Pi_r)$ when a pure CO_2 discharge is ignited at $p = 5$ Torr and $I = 50$ mA at Mars and Earth background temperatures. The reactions are identified in Table 1.

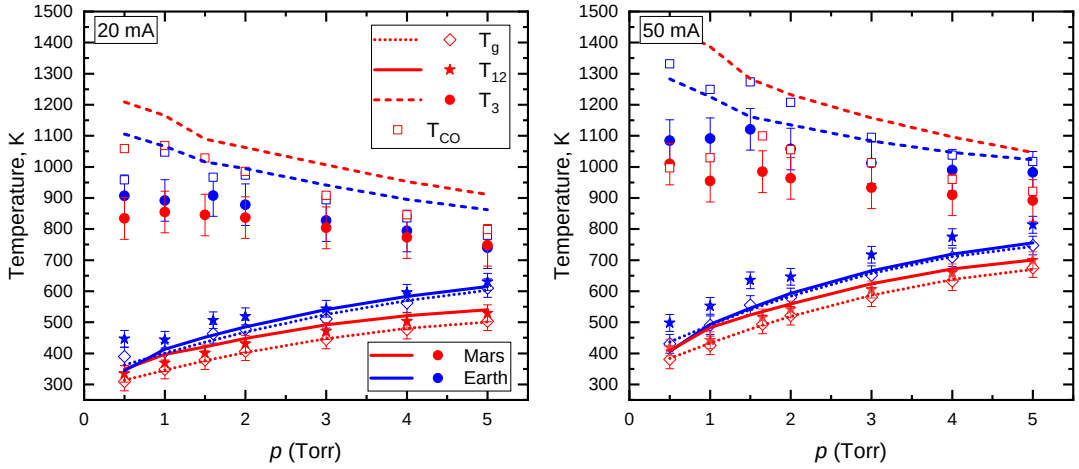

Figure 11. Experimental value of the gas temperature T_g ($\cdot \diamond \cdot$), together with the measured (symbols) and calculated (lines) vibrational temperatures of the asymmetric stretching mode T_3 ($\bullet$, $--$) and the common temperature of the bending and symmetric modes T_{12} ($\star$, —) and CO vibrational temperature T_{CO} (*square*), when a pure CO_2 discharge is ignited at Mars and Earth background temperatures at currents $I = 20$ mA (left panel) and $I = 50$ mA (right panel).

It contributes about 1% to the destruction of the $CO(a\ ^3\Pi_r)$ state, but its actual importance should not be underestimated, as it brings an exit path from the CO manifold.

It is worth noting the prevalence of processes involving electronically excited states, $O_2(a\ ^1\Delta_g)$, $O_2(b\ ^1\Sigma_g^+)$, $O(^1D)$ and $CO(a\ ^3\Pi_r)$, in the overall kinetics. This remark is particularly striking for the cases of $O(^1D)$ and $CO(a\ ^3\Pi_r)$, whose relative densities are rather low, as it can be seen in Figure 7. Nonetheless, the results reveal a strong coupling between the kinetics of all these electronically excited states and the parent atoms and molecules. Similar conclusions have been drawn for oxygen plasmas in [60]. A more detailed analysis of the plasma chemistry in CO_2-containing discharges will be presented in future publications.

4.2. CO_2 vibrational kinetics at Mars and Earth temperature conditions

One argument advanced in [24, 25] in favor of ISRU on Mars by plasmas was the increased degree of vibrational non-equilibrium that would be promoted by the ambient conditions on the red planet. In appropriate discharge configurations, such as radio-frequency, microwave or gliding arc discharges, it might be possible to benefit from the energy stored in the vibrational levels to enhance the energy efficiency of CO_2 dissociation [12]. In the DC glow discharges under study, CO_2 dissociation proceeds mainly by direct electron impact, with a small to negligible contribution from purely vibrational mechanisms [40, 67]. Nevertheless, it is very instructive to verify the validity of the conjecture in [24, 25], to guide the development of plasmas sources designed for ISRU on Mars, as well as to further analyze the results in Figure 4.

Figure 11 represents the measured gas temperature, T_g, the vibrational temperature of

the asymmetric stretching mode, T_3, the common temperature of the bending and symmetric stretching modes, T_{12}, and the vibrational temperature of CO, T_{CO}, together with the model predictions for CO_2 "vibrational temperatures." The CO vibrational temperature is taken into account as an input parameter for the EEDF calculation, but CO vibrations are not accounted for in the chemistry module and, thus, are not calculated in the model. It is worth emphasizing that the current state-to-state model provides the populations of the individual vibrational levels of the CO_2 molecules. Therefore, the "vibrational temperatures" correspond to the fitting of the individual populations to Treanor distributions. Moreover, the fact that the bending and symmetric stretching modes can be described by a common "temperature" in these conditions is not an imposition of the model but rather an outcome of the simulations, as also pointed out in [36]. Additional details on the fitting of the individual populations to the corresponding distributions are given in [35,36], where some vibrational distribution functions are presented. The simulations describe satisfactorily the trend and magnitude of the observed T_{12} and T_3, whose values do not change significantly from a discharge ignited in Martian or Earthly ambient temperatures. The model predicts a slightly larger vibrational temperature of the asymmetric stretching mode on Mars than on Earth, that is not confirmed experimentally. This discrepancy is likely due to the simplified vibrational kinetics considered here concerning energy transfers between CO_2 and the dissociation products, O, O_2 and CO, that only accounts for very few VT collisions of vibrationally excited CO_2 with O atoms and disregards collisions with O_2 and CO (see section 3). In any case, the main effects seem to be already captured with the present model. The variations of T_3 with pressure and current are similar to the ones reported and discussed in detail by Morillo-Candas [66] for Earth conditions. They further confirm the interest of the Martian pressure range to benefit from vibrational non-equilibrium to decompose CO_2.

One interesting phenomenon revealed by Figure 11 is a small increase of the degree of vibrational non-equilibrium when passing from Earth to Mars, as predicted theoretically in [24]. This effect is more clearly exhibited in Figure 12, which shows the ratios T_3/T_g and T_{12}/T_g, characterizing the degree of non-equilibrium in the plasma [24, 25]. It can be verified that the common temperature of the bending and symmetric stretching modes remains always nearly in equilibrium with the gas temperature. On the contrary, the asymmetric stretching mode, of major interest for vibrationally-driven dissociation [12], is clearly out of equilibrium, with a bigger departure from equilibrium in Martian conditions than on Earth, but only for the lower current, $I = 20$ mA. In this case, the ratio T_3/T_g is always $25 - 30\%$ higher on Mars than on Earth. This behavior is the outcome of the enhanced up-pumping along the asymmetric stretching mode as the temperature decreases,

$$CO_2(00^0\nu_3) + CO_2(00^0\nu_3') \rightleftharpoons CO_2(00^0(\nu_3 + 1)) + CO_2(00^0(\nu_3' - 1)) \,,$$

since in the present temperature domain this VV interaction is dominated by long-range attractive forces [68], and of the decrease of the deactivation in VT mechanisms, dominated by short range repulsive forces. A somewhat similar effect is predicted from the model for $I = 50$ mA but is not confirmed experimentally. As noted above, these differences might stem from the simplified vibrational kinetics included in the model.

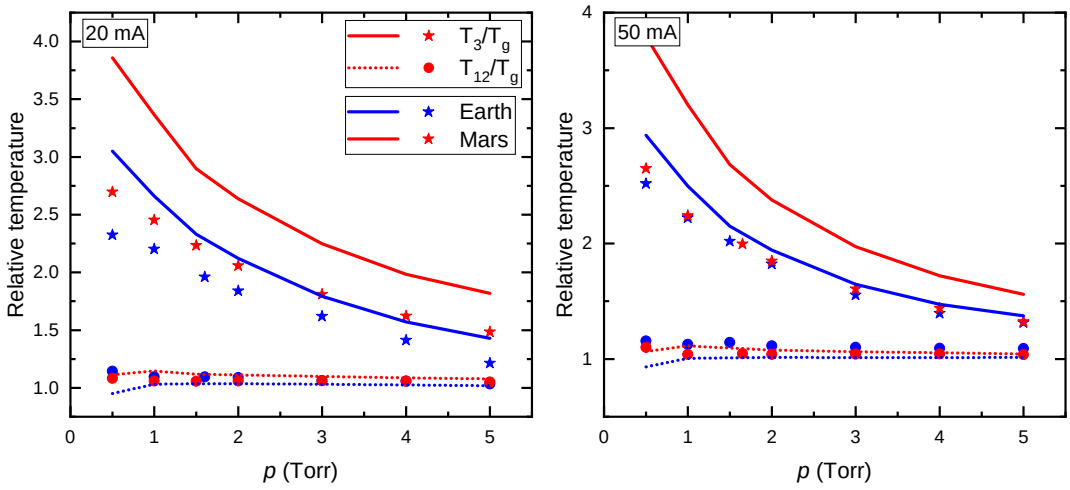

Figure 12. Measured (symbols) and calculated (lines) ratios T_3/T_g (—,⋆) and T_{12}/T_g (···, •) when a pure CO_2 discharge is ignited at Mars and Earth background temperatures at currents $I = 20$ mA (left panel) and $I = 50$ mA (right panel).

4.3. Synthetic Martian atmosphere

This section addresses the experimental investigation of the influence of the minor constituents of the Martian atmosphere, Ar and N_2, on the plasma properties and CO_2 decomposition. Experiments are carried-out in pure CO_2 and in 96%CO_2-2%Ar-2%N_2 plasmas, with a gas flow $\Phi = 19.25$ sccm, ignited both in Mars and Earth input gas temperatures. It has been speculated that the presence of traces of Ar and N_2 could be beneficial for the production of oxygen and carbon monoxide by enhancing CO_2 plasma dissociation [24, 25], but no experimental evidence has been presented to date.

The measured values of the reduced electric field are shown in Figure 13, the temperatures T_g, T_{12} and T_3 in Figure 14, the temperature ratios T_3/T_g, T_{12}/T_g and T_3/T_{12} in Figure 15, and the dissociation fraction α in Figure 16. Figures 13-15 indicate that the presence of Ar and N_2 in the Martian atmosphere has a negligible effect on the reduced field and on the vibrational temperatures, maintaining a significant degree of non-equilibrium. Even though, a small but consistent positive influence on the production of CO from CO_2 is visible in Figure 16, despite some fluctuation of the results and the outlier data on Earth at $p \leq 2$ Torr and $I = 50$ mA. It is worth noting that the decomposition here is lower than what is reported in figure 4. This is due to the lower residence times of the gas in the plasma, which decrease ∼3 times as the flow increases.

The reasons for a favorable effect of traces of N_2 and Ar in CO_2 decomposition are most likely due to the modifications induced by Ar and N_2 in the EEDF and by the small variations in E/N. Figure 17 shows the EEDFs calculated for the experimental conditions of reduced field, E/N, common vibrational temperature of the symmetric stretching and bending modes, T_{12}, vibrational temperatures of the asymmetric stretching mode, T_3, and of CO, T_{CO},

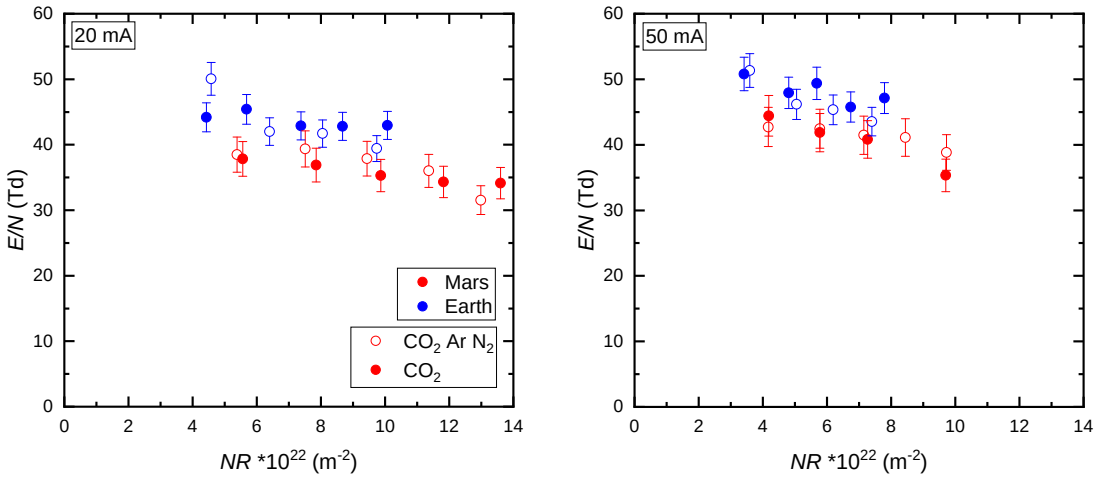

Figure 13. Reduced electric field, E/N, as a function of the NR product, measured when pure CO_2 (•) and 96%CO_2-2%Ar-2%N_2 (∘) discharges are ignited at Mars and Earth background temperatures at currents $I = 20$ mA (left panel) and $I = 50$ mA (right panel).

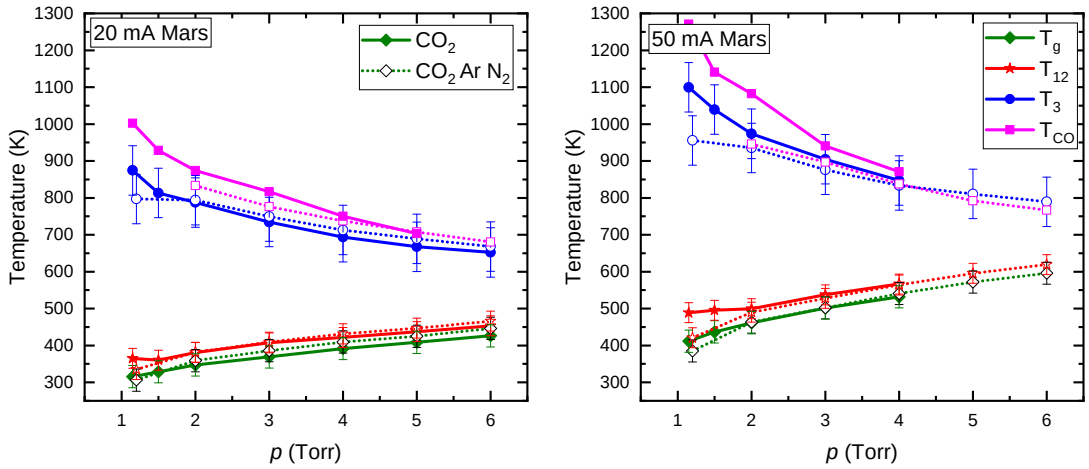

Figure 14. Experimental values of the gas temperature T_g (◆, ◇), the vibrational temperature of the asymmetric stretching mode T_3 (●, ∘) and the common vibrational temperature of the bending and symmetric modes T_{12} (★, ☆) and CO vibrational temperature T_{CO} (■,□), when pure CO_2 (—, closed symbols) and 96%CO_2-2%Ar-2%N_2 (···, open symbols) discharges are ignited at Mars background temperature at currents $I = 20$ mA (left panel) and $I = 50$ mA (right panel).

for a discharge ignited at Mars background temperature, current $I = 50$ mA and pressures $p = 3$ Torr and $p = 5$ Torr, in pure CO_2 and in a synthetic Martian atmosphere 96%CO_2-2%Ar-2%N_2. The vibrational temperature of N_2 was assumed to be the same as T_{CO}. Figure 17 shows an enhancement of the tail of the EEDF for the Martian mixture in the region of energies around 7 eV, the energy threshold for dissociation [29, 59], which leads to a higher electron impact dissociation rate coefficient. The effect is specially noticeable for $p = 5$ Torr, where the observed increase in the dissociation fraction is higher, and is due to the differences

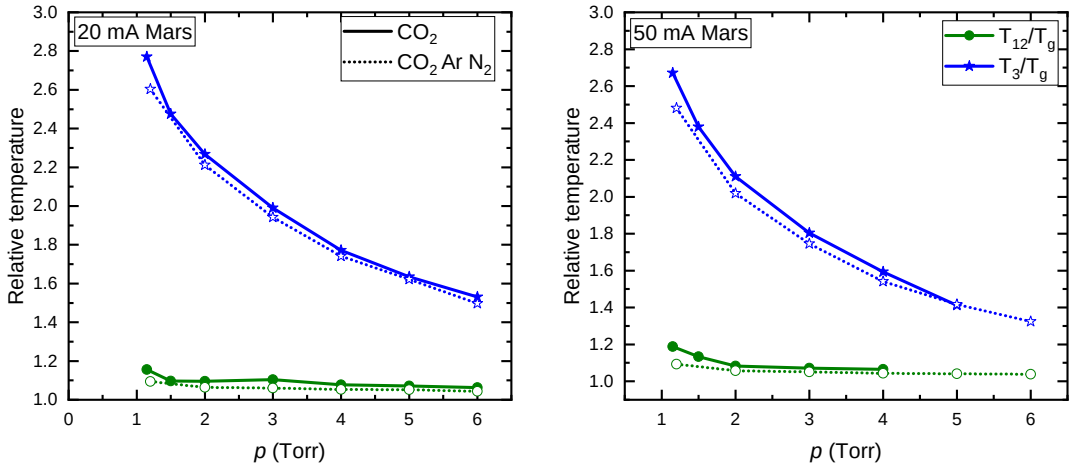

Figure 15. Experimental values of the ratios T_3/T_g (★, ☆) and T_{12}/T_g (●, ○), when pure CO_2 (—, closed symbols) and 96%CO_2-2%Ar-2%N_2 (···, open symbols) discharges are ignited at Mars background temperature at currents $I = 20$ mA (left panel) and $I = 50$ mA (right panel).

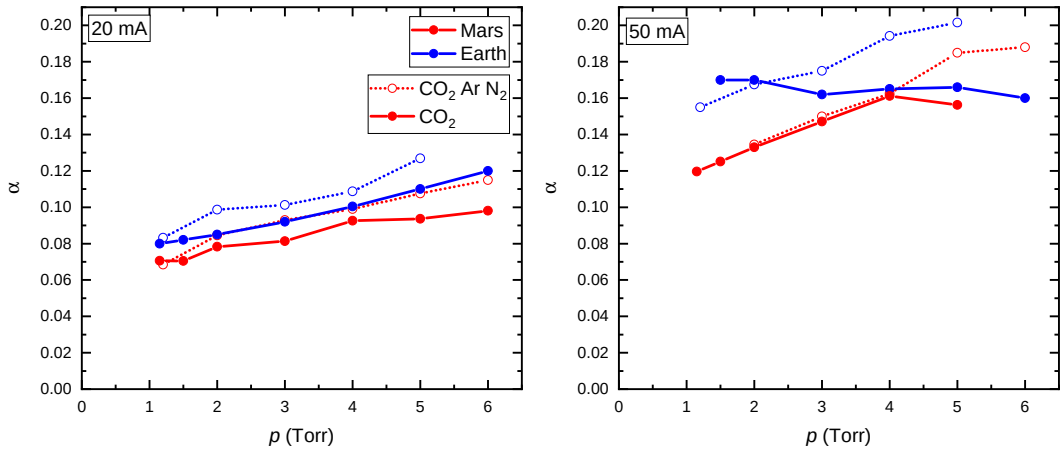

Figure 16. Experimental CO_2 dissociation fraction when pure CO_2 (-●-) and 96%CO_2-2%Ar-2%N_2 (· ∘ ·) discharges are ignited at Mars and Earth background temperatures at currents $I = 20$ mA (left panel) and $I = 50$ mA (right panel)

in the cross sections between the different gases and to a small increase in the values of E/N when passing from pure CO_2 to CO_2-Ar-N_2 (from 41.9 Td to 42.5 Td at 3 Torr, and from 35.3 Td to 41.1 Td at 5 Torr). Two subtle but identifiable positive effects are the presence of Ar, that shifts the EEDF to higher energies [69], and the vibrational temperature of N_2, that enhances the high energy tail via electron superelastic collisions with vibrationally excited nitrogen.

Another possibility for a positive influence of N_2 would be the transfer of vibrational energy from nitrogen to the asymmetric stretching mode of CO_2 and the enhancement of dissociation via the purely vibrational mechanism [12]. Notwithstanding, the measured vibrational temperatures are not significantly affected and, in addition, the purely vibrational

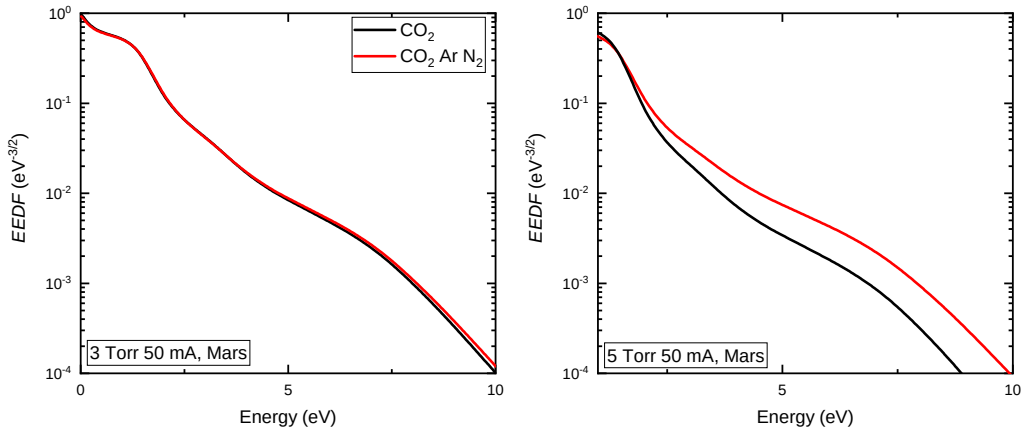

Figure 17. Electron Energy Distribution Functions calculated for the experimental values of E/N, T_{12}, T_3 and T_{CO} at $p = 3$ Torr (left panel) and $p = 5$ Torr (right panel), $I = 50$ mA, and Mars input gas temperature, for pure CO_2 (—) and 96%CO_2-2%Ar-2%N_2 (—).

mechanism does not seem to play a significant role in the present conditions. Note, however, that the measured vibrational "temperatures" are only representative of the populations of the lower vibrational levels and do not bring any information regarding the populations of the higher ones, which may deviate from equilibrium Boltzmann distributions and be modified by the presence of N_2. A positive effect of N_2 addition was also observed in recent experiments [41, 70], reinforcing the suggestion from Figure 17 that the answer to why the CO yield is higher in synthetic Martian atmosphere than in pure CO_2 plasmas may lay in the CO_2-N_2 kinetics. Further research is necessary to elucidate the origin this effect.

5. Conclusions

This work presents an experimental and modeling investigation on the potential of low-temperature plasmas for *in situ* resource utilization (ISRU) on Mars. The research focus on the decomposition of CO_2, which is freely abundant in the Martian atmosphere and creates the building blocks for the local production of oxygen and fuels.

DC glow discharges operating at pressures in the range 0.5-5 Torr are ignited in pure CO_2 and in a synthetic Martian atmosphere composed of 96%CO_2-2%Ar-2%N_2, discharge currents $I = 20 - 50$ mA, with the input gas either at Martian ($\sim$ 220 K) or Terrestrial ($\sim$ 300 K) temperatures. The CO_2 and CO vibrational temperatures and the CO and CO_2 concentrations are measured, providing an experimental characterization of plasmas created in conditions realistically mimicking the atmosphere of Mars.

In the system under study, CO_2 is essentially decomposed by direct electron impact, both on molecules in the vibrational ground-state (00^00) and in vibrational excited states. The contribution of the latter sates comes mainly from the lower-laying levels (01^10), (02^20) and ($10^00 + 02^00$), with several other levels having contributions of a few percent. Dissociation fractions up to 30% are observed, a very encouraging result considering that the present setup

is designed for fundamental studies and is far from suited for the development a prototype.

The plasma chemistry is significantly influenced by electronically excited states, such as $O_2(a\,^1\Delta_g)$, $O_2(b\,^1\Sigma_g^+)$, $O(^1D)$ and $CO(a\,^3\Pi_r)$. Therefore, a full control and optimization of the plasma requires a detailed understanding of the strongly coupled kinetics of these states.

The results confirm that the Martian conditions of temperature and pressure pump the asymmetric stretching vibration mode and lead to a stronger degree of non-equilibrium than on Earth, believed to have a positive influence in dissociation [12]. For the current discharge configuration, dissociation is driven by electron impact and the conversion factor at low temperature is slightly lower than at room temperature. Nevertheless, vibrational kinetics has a very significant influence in dissociation as a result of electron superelastic collisions with vibrationally excited CO and CO_2 molecules, that modify the electron energy distribution function and lead to an increase of the electron impact dissociation rate coefficients and, accordingly, of CO production. Atomic oxygen is a strong quencher of vibrationally excited CO_2 and has also an important effect in shaping the vibrational distribution functions.

The new experimental data corroborate the conjecture of a positive effect of the Martian atmospheric composition on dissociation advanced in paper [24, 25]. This behavior is most likely related to modifications in the electron kinetics induced by the presence of nitrogen and argon and the associated enhanced dissociation by electron impact.

Despite the beneficial effects of the low ambient temperature and of the presence of Ar and N_2 in the Martian atmosphere, their impact on CO_2 decomposition is relatively small. Indeed, the results obtained for Mars and Earth background temperatures, as well as for pure CO_2 and for the synthetic Martian atmosphere, are rather similar in what concerns the identification of the main creation/destruction mechanisms and all the trends observed. Thus, knowledge on the energy-transfer pathways acquired on Earth can, to a very considerable extent, be transposed to Mars.

The present results establish experimental evidence of the feasibility of oxygen and propellant production by plasma decomposition of CO_2 from the Martian atmosphere and suggest the possible development of more sophisticated setups that can take fully advantage of non-equilibrium and/or promote dissociation by electron impact. Future research should concentrate on the design and optimization of robust and efficient plasma sources and on the procedure to separate O_2 from the other dissociation products. Recent proposals for product separation include the use of silver membranes by Premathilake *et al* [17] and a new electrochemical membrane reactor presented by Goede and co-workers [71, 72].

It is worth noticing that emerging plasma technologies for CO_2 reforming on Earth are already expected to be competitive with solid oxide electrolysis (SOEC) [73–75], the technology proposed in NASA's MOXIE program. Therefore, a plasma-electrochemical process will most certainly be a viable alternative to SOEC for oxygen production on Mars. In fact, the efficiency of SOEC is likely to decrease as compared to that on Earth, because extra energy is necessary to compress the gas up to 1 atm, pre-heat it up to 1100 K and cool down the exhaust stream [9, 10]. Furthermore, sophisticated thermal insulation systems are mandatory. In turn, the efficiency of plasma dissociation of CO_2 on Mars is likely to increase as compared to that on Earth, due to the beneficial effects demonstrated in this paper and the absence of

vacuum pumps. A conservative estimation can be made as follows. Consider a thermodynamic value of $\sim 50\%$ energy efficiency for gas phase dissociation, as reached recently by den Harder *et al* [74], marginally amplified by the interaction with catalytic walls and membrane to about 55%. At 300 W it corresponds to the production of 35 g of O_2 per hour, at an energy cost of 10 eV/molecule. A decrease in performance of about 50%, to account for unexpected difficulties and the uncertainties of development of a new technology, brings these numbers to approximately 20 g of O_2 per hour, at an energy cost of 18 eV per molecule and 31% energy efficiency. These rather prudent values outperform the most optimistic predictions of MOXIE by 100%. Furthermore, considering the typical design of a microwave reactors described in [73, 74, 76] and following the analysis by Raposo in [77], a competitive MW prototype can be assembled. The main constituents of a microwave plasma reactor are the microwave generator, the isolator, the impedance tuner, the reactor vessel and the waveguide [76]. A solid-state microwave generator of 2.45 GHz with an output power of 500 W (LEANGEN-2450M-500-M) is enough to ignite the plasma at the same power as MOXIE and compatible with the solar and wind tested power generation on Mars. This device adds up to a total of ~ 1.3 Kg. By designing this prototype to work at the unique conditions on Mars, especially the pressure of 4.5 Torr, there is no need to use a tuner and a waveguide of 86.5 mm and antenna are sufficient to conduct the microwave power in order to maximise the field strength. By using a light material as Aluminium, a 500 g system can be assembled. Finally, for the reactor vessel a 300 g quartz tube can be used due to its permeability to the microwaves. The isolator components, also made from Aluminium, can be estimated to weight 0.6 Kg (0.22 m^3), having enough margin for adjustments and extra shielding options. Such compact microwave reactor ($25 \times 20 \times 5$ cm) weights less than 3 Kg versus the 15 Kg of MOXIE. These estimations of oxygen yield and weight of the prototype bring further evidence in favor of the plausibility and significance of plasma ISRU on Mars as a complementary technology to SOEC.

Acknowledgments

This work was partially funded by Portuguese FCT - Fundação para a Ciência e a Tecnologia, under projects UIDB/50010/2020 and UIDP/50010/2020 and grant PD/BD/114398/2016 (PD-F APPLAuSE).

References

[1] NASA, "Chronology of Mars Exploration," 2020.

[2] R. M. Haberle, "Solar System/Sun, Atmospheres, Evolution of Atmospheres. Planetary Atmospheres: Mars," in *Encyclopedia of Atmospheric Sciences*, vol. 5, pp. 168–177, Elsevier, 2^{nd} ed., 2015.

[3] R. L. Ash, W. L. Dowler, and G. Varsi, "Feasibility of rocket propellant production on mars," *Acta Astronaut.*, vol. 5, pp. 705–724, 1978.

[4] M. L. Stancati, J. C. Niehoff, W. C. Wells, and R. L. Ash, "Hybrid rocket propulsion and in-situ propellant production for future mars missions," in *Conference on Advanced Technology for Future Space Systems*, (Hampton, VA), p. 906, 1979.

[5] G. A. Landis and D. L. Linne, "Mars Rocket Vehicle Using In Situ Propellants," *Journal of Spacecraft and Rockets*, vol. 38, no. 5, pp. 730–735, 2001.

[6] A. J. Boiron and B. J. Cantwell, "Hybrid rocket propulsion and in-situ propellant production for future mars missions," in *49th AIAA/ASME/SAE/ASEE Joint PropulsionConference*, (San Jose, CA), p. 3899, 2013.

[7] G. B. Sanders, A. Paz, L. Oryshchyn, and K. Araghi, "Mars ISRU for Production of Mission Critical Consumables – Options , Recent Studies , and Current State of the Art," *SPACE Conferences and Exposition*, pp. 1–14, 2015.

[8] J. J. Hartvigsen, S. Elangovan, D. Larsen, J. Elwell, M. Bokil, L. Frost, and L. M. Clark, "Challenges of solid oxide electrolysis for production of fuel and oxygen from mars atmospheric CO_2," *ECS Transactions*, vol. 68, pp. 3563–3583, 2015.

[9] M. H. Hecht, D. R. Rapp, and J. A. Hoffman, "The Mars Oxygen ISRU experiment (MOXIE)," in *International Workshop on Instrumentation for Planetary Missions*, (Greenbelt, MD), p. 1134, 2014.

[10] M. H. Hecht and J. A. Hoffman, "The mars oxygen ISRU experiment (MOXIE) on the mars 2020 rover," in *3rd International Workshop on Instrumentation for Planetary Missions*, (Pasadena, CA), p. 4130, 2016.

[11] IEA, "Global energy & CO_2 status report 2019." International Energy Agency, https://www.iea.org/reports/global-energy-co2-status-report-2019, 2019.

[12] A. Fridman, *Plasma Chemistry*. Cambridge University Press, 2008.

[13] A. Goede and R. van de Sanden, "CO_2 neutral fuels," *EPN*, vol. 47/3, pp. 22–25, 2017.

[14] R. A. Outlaw, "O_2 and CO_2 glow-discharge-assisted oxygen transport through Ag," *J. Appl. Phys.*, vol. 68, pp. 1002–1004, 1990.

[15] R. L. Ash, D. Wu, and R. A. Outlaw, "A study of glow-discharge and permeation techniques for extraterrestrial oxygen beneficiation," *Adv. Space Res.*, vol. 14, pp. (6)259–(6)263, 1994.

[16] D. Wu, R. A. Outlaw, and R. L. Ash, "Extraction of oxygen from CO_2 using glow-discharge and permeation techniques," *J. Vac. Sci. Technol. A*, vol. 14, pp. 408–414, 1996.

[17] D. Premathilake, R. A. Outlaw, R. A. Quinlan, and C. E. Byvik, "Oxygen generation by carbon dioxide glow discharge and separation by permeation through ultrathin silver membranes," *Earth and Space Science*, 2019.

[18] J. Gruenwald, "A proposal for a plasma technology based hybrid life support system for future Mars habitats," *J. Space Technol.*, vol. 4, pp. 1–6, 2014.

[19] H. L. K. Manning, I. L. ten Kate, S. J. Battel, and P. R. Mahaff, "Electric discharge in the martian atmosphere, Paschen curves and implications for future missions," *Adv. Space Res.*, vol. 46, pp. 13340–1340, 2010.

[20] G. Garcia-Cosio, H. Martinez, M. Calixto-Rodriguez, and A. Gomez, "DC discharge experiment in an Ar/N_2/CO_2 ternary mixture: A laboratory simulation of the martian ionosphere's plasma environment," *JQSRT*, vol. 112, pp. 2787–2793, 2011.

[21] J. Annaloro and A. Bultel, "Vibrational and electronic collisional-radiative model in CO_2-N_2-Ar mixtures for mars entry problems," *Phys. Plasmas*, vol. 26, p. 103505, 2019.

[22] A. Laricchiuta, D. Bruno, M. Capitelli, C. Catalfamo, R. Celiberto, G. Colonna, P. Diomede, D. Giordano, C. Gorse, S. Longo, D. Pagano, and F. Pirani, "High temperature Mars atmosphere. Part I: transport cross sections," *Eur. Phys. J. D*, vol. 54, pp. 607–612, 2009.

[23] C. Catalfamo, D. Bruno, G. Colonna, A. Laricchiuta, and M. Capitelli, "High temperature Mars atmosphere. Part II: transport properties," *Eur. Phys. J. D*, vol. 54, pp. 613–621, 2009.

[24] V. Guerra, T. Silva, P. Ogloblina, M. Grofulović, L. Terraz, M. Lino da Silva, C. D. Pintassilgo, L. L. Alves, and O. Guaitella, "The case for in situ resource utilisation for oxygen production on Mars by non-equilibrium plasmas," *Plasma Sources Sci. Technol.*, vol. 26, p. 11LT01, 2017.

[25] V. Guerra, T. Silva, and O. Guaitella, "Living on Mars: how to produce oxygen and fuel to get home," *EPN*, vol. 49/2, pp. 15–18, 2018.

[26] B. L. M. Klarenaar, R. Engeln, D. C. M. van den Bekerom, M. C. M. van de Sanden, A. S. Morillo-Candas, and O. Guaitella, "Time evolution of vibrational temperatures in a CO_2 glow discharge measured with infrared absorption spectroscopy," *Plasma Sources Sci. Technol.*, vol. 26, p. 115008, 2017.

[27] A. S. Morillo-Candas, C. Drag, J. P. Booth, T. C. Dias, V. Guerra, and O. Guaitella, "Oxygen atom kinetics in CO_2 plasmas ignited in a DC glow discharge," *Plasma Sources Sci. Technol.*, vol. 28, p. 075010, 2019.

[28] P. Ogloblina, V. Guerra, A. S. Morillo-Candas, and O. Guaitella, "Plasma reforming for oxygen production

on mars," in *8th European Conference for Aeronautics and aero-Space Sciences (EUCASS)*, 2019.

[29] M. Grofulović, L. L. Alves, and V. Guerra, "Electron-neutral scattering cross sections for CO_2: a complete and consistent set and an assessment of dissociation," *J. Phys. D: Appl. Phys.*, vol. 49, p. 395207, 2016.

[30] P. Ogloblina, A. Tejero-del-Caz, V. Guerra, and L. L. Alves, "Electron impact cross sections for carbon monoxide and their importance in the electron kinetics of CO_2–CO mixtures," *Plasma Sources Sci. Technol.*, vol. 29, p. 015002, 2020.

[31] A. Tejero-del-Caz, V. Guerra, D. Gonçalves, M. Lino da Silva, L. Marques, N. Pinhão, C. D. Pintassilgo, and L. L. Alves, "The LisbOn KInetics Boltzmann solver," *Plasma Sources Sci. Technol.*, vol. 28, p. 043001, 2019.

[32] V. Guerra and J. Loureiro, "Kinetic model of a low pressure microwave discharge in O_2-N_2 including the effects of O^- ions on the characteristics for plasma maintenance," *Plasma Sources Sci. Technol.*, vol. 6, pp. 373–385, 1999.

[33] A. Tejero-del-Caz, L. L. Alves, V. Guerra, D. Gonçalves, M. Lino da Silva, N. Pinhão, L. Marques, and C. D. Pintassilgo, "The LisbOn KInetics tool suit," in *71st Annual Gaseous Electronics Conference*, (Portland, OR), p. GT1.071, 2018.

[34] "The LisbOn KInetics - LoKI," 2019.

[35] T. Silva, M. Grofulović, B. L. M. Klarenaar, O. Guaitella, R. Engeln, C. D. Pintassilgo, and V. Guerra, "Kinetic study of CO_2 plasmas under non-equilibrium conditions. I. Relaxation of vibrational energy," *Plasma Sources Sci. Technol.*, vol. 27, p. 015019, 2018.

[36] M. Grofulović, T. Silva, B. L. M. Klarenaar, A. S. Morillo-Candas, O. Guaitella, R. Engeln, C. D. Pintassilgo, and V. Guerra, "Kinetic study of CO_2 plasmas under non-equilibrium conditions. II. Input of vibrational energy," *Plasma Sources Sci. Technol.*, vol. 27, p. 015009, 2018.

[37] T. Silva, M. Grofulović, L. Terraz, C. D. Pintassilgo, and V. Guerra, "Modelling the input and relaxation of vibrational energy in CO_2 plasmas," *J. Phys. D: Appl. Phys.*, vol. 51, p. 464001, 2018.

[38] T. Silva, M. Grofulović, L. Terraz, C. D. Pintassilgo, and V. Guerra, "Dynamics of gas heating in the afterglow of pulsed CO_2 and CO_2-N_2 glow discharges at low pressure," *Plasma Chem. Plasma Process.*, 2020.

[39] A. F. Silva, A. S. Morillo-Candas, A. Tejero-del-Caz, L. L. Alves, O. Guaitella, and V. Guerra, "A reaction mechanism for vibrationally cold CO_2 plasmas," *Plasma Sources Sci. Technol.*, 2020.

[40] A. S. Morillo-Candas, T. Silva, B. L. M. Klarenaar, M. Grofulović, V. Guerra, and O. Guaitella, "Electron impact dissociation of CO_2," *Plasma Sources Sci. Technol.*, vol. 29, p. 01LT01, 2020.

[41] L. Terraz, T. Silva, A. Morillo-Candas, O. Guaitella, A. Tejero-del-Caz, L. L. Alves, and V. Guerra, "Influence of N_2 on the CO_2 vibrational distribution function and dissociation yield in non-equilibrium plasmas," *J. Phys. D: Appl. Phys.*, vol. 53, p. 094002, 2020.

[42] Y. P. Raizer, *Gas discharge physics*. Springer-Verlag, 1991.

[43] B. L. M. Klarenaar, A. S. Morillo-Candas, M. Grofulović, M. C. M. van de Sanden, R. Engeln, and O. Guaitella, "Excitation and relaxation of the asymmetric stretch mode of CO_2 in a pulsed glowdischarge," *Plasma Sources Sci. Technol.*, vol. 28, p. 035011, 2019.

[44] L. L. Alves, P. Coche, M. A. Ridenti, and V. Guerra, "Electron scattering cross sections for the modelling of oxygen-containing plasmas," *Eur. Phys. J. D*, vol. 70, p. 124, 2016.

[45] "Plasma data exchange project," 2010.

[46] J. . Lowke, A. V. Phelps, and B. W. Irwin, "Predicted electron transport coefficients and operating characteristics of CO_2-N_2-He laser mixtures," *J. Appl. Phys.*, vol. 44, p. 4664, 1973.

[47] R. Celiberto, V. Laporta, A. Laricchiuta, J. Tennyson, and J. M. Wadehra, "Molecular physics of elementary processes relevant to hypersonics: Electron-molecule collisions," *Open Plasma Phys. J.*, vol. 7 (suppl 1:M2), pp. 33–47, 2014.

[48] R. Celiberto, I. Armenise, M. Cacciatore, M. Capitelli, F. Esposito, P. Gamallo, R. K. Janev, A. Laganà, V. Laporta, A. Laricchiuta, A. Lombardi, M. Rutigliano, R. Sayós, J. Tennyson, and J. M. Wadehra, "Atomic and molecular data for spacecraft re-entry plasmas," *Plasma Sources Sci. Technol.*, vol. 25, p. 033004, 2016.

[49] Y. Itikawa, "Cross sections for electron collisions with carbon monoxide," *J. Phys. Chem. Ref. Data*, vol. 44,

p. 013105, 2015.

[50] V. Laporta, C. M. Cassidy, J. Tennyson, and R. Celiberto, "Electron-impact resonant vibration excitation cross sections and rate coefficients for carbon monoxi," *Plasma Sources Sci. Technol.*, vol. 21, p. 045005, 2012.

[51] T. Sawada, D. L. Sellin, and A. E. S. Green, "Electron impact excitation cross sections and energy degradation in CO," *J. Geophys. Res.*, vol. 77, no. 25, pp. 4819–28, 1972.

[52] D. Rapp and D. D. Briglia, "Total cross sections for ionization and attachment in gases by electron impact. II. Negative-ion formation," *J. Chem. Phys.*, vol. 43, no. 5, pp. 1480–1489, 1965.

[53] D. Rapp and P. Englander-Golden, "Total cross sections for ionization and attachment in gases by electron impact. I. Positive ionization," *J. Chem. Phys.*, vol. 43, pp. 1464–1479, 1965.

[54] P. C. Cosby, "Electron-impact dissociation of carbon monoxide," *J. Chem. Phys.*, vol. 98, no. 10, pp. 7804–7818, 1993.

[55] A. V. Phelps, "Tabulations of collision cross sections and calculated transport and reaction coefficients for electron collisions with O_2," Tech. Rep. 28, JILA Information Center Report, 1985. University of Colorado, Boulder, Colorado, USA.

[56] S. A. Lawton and A. V. Phelps, "Excitation of the $b^1\Sigma_g^+$ state of O_2 by low energy electrons," *J. Chem. Phys.*, vol. 69, p. 1055, 1978.

[57] R. R. Laher and F. R. Gilmore, "Updated excitation and ionization cross sections for electron impact on atomic oxygen," *J. Phys. Chem. Ref. Data*, vol. 19, p. 277, 1990.

[58] V. Guerra and J. Loureiro, "Electron and heavy particle kinetics in a low pressure nitrogen glow discharge," *Plasma Sources Sci. Technol.*, vol. 6, pp. 361–372, 1997.

[59] L. S. Polak and D. I. Slovetsky, "Electron impact induced electronic excitation and molecular dissociation," *Int. J. Radiat. Phys. Chem.*, vol. 8, pp. 257–282, 1976.

[60] A. Annušová, D. Marinov, J. P. Booth, N. Sirse, M. Lino da Silva, B. Lopez, and V. Guerra, "Kinetics of highly vibrationally excited O_2(X) molecules in inductively-coupled oxygen plasmas," *Plasma Sources Sci. Technol.*, vol. 27, p. 045006, 2018.

[61] A. S. Morillo-Candas, B. L. M. Klarenaar, C. Amoedo, V. Guerra, and O. Guaitella, "Effect of oxygen atoms on the vibrational kinetics of CO_2 and CO revealed by the use of a large surface area material," *J. Phys. D: Appl. Phys.*, 2020.

[62] M. López-Puertas, R. Rodrigo, J. J. López-Moreno, and F. W. Taylor, "A non-LTE radiative transfer model for infrared bands in the middle atmosphere. II. CO_2 (2.7 and 4.3 μm) and water vapour (6.3 μm) bands and N_2(1) and O_2(1) vibrational levels," *J. Atmospheric Terr. Phys.*, vol. 48, pp. 749–746, 1986.

[63] K. Shofield, "Critically evaluated rate constants for gaseous reactions of several electronically excited species," *J. Phys. Chem. Ref. Data*, vol. 8, pp. 723–798, 1979.

[64] V. Guerra, E. Tatarova, F. M. Dias, and C. M. Ferreira, "On the self-consistent modeling of a traveling wave sustained nitrogen discharge," *J. Appl. Phys.*, vol. 91, pp. 2648–2661, 2002.

[65] L. D. Pietanza, G. Colonna, and M. Capitelli, "Self-consistent electron energy distribution functions, vibrational distributions, electronic excited state kinetics in reacting microwave CO_2 plasma: An advanced model," *Phys. Plasmas*, vol. 27, p. 023513, 2020.

[66] A. S. Morillo-Candas, *Investigation of fundamental mechanisms of CO_2 plasmas*. Phd thesis, Ecole Polytechnique - Université Paris-Saclay, 2019.

[67] A. S. Morillo-Candas, V. Guerra, and O. Guaitella, "Time evolution of the dissociation fraction in RF CO_2 plasmas: impact and nature of back reaction mechanisms," *Plasma Sources Sci. Technol.*, 2020.

[68] R. T. Pack, "Analytic estimation of almost resonant molecular energy transfer due to multipolar potentials. VV processes involving CO_2," *J. Chem. Phys.*, vol. 72, pp. 6140–6152, 1980.

[69] A. Janeco, N. R. Pinhão, and V. Guerra, "Electron kinetics in He/CH_4/CO_2 mixtures used for methane conversion," *J. Phys. Chem. C*, vol. 119, pp. 109–120, 2015.

[70] M. Grofulović, B. L. M. Klarenaar, O. Guaitella, V. Guerra, and R. Engeln, "A rotational Raman study under non-thermal conditions in pulsed CO_2-N_2 and CO_2-O_2 glow discharges," *Plasma Sources Sci. Technol.*, vol. 28, p. 045014, 2019.

[71] A. P. H. Goede, "CO_2 neutral fuels," *EPJ Web Conf.*, vol. 189, p. 00010, 2018.

[72] A. Pandiyan, D. Neagu, V. Kyriakou, R. Sharma, V. Middelkoop, S. Weber, A. Goede, S. Welzel, and M. Tsampas, "Electrochemical membrane reactor for oxygen separation after CO_2 plasmolysis," in *14th International Conference on Catalysis in Membrane Reactors (ICCMR-14)*, 2019.

[73] G. J. van Rooij, D. C. M. van den Bekerom, N. den Harder, T. Minea, G. Berden, W. A. Bongers, R. Engeln, M. F. Graswinckel, E. Zoethout, and M. C. M. van de Sanden, "Taming microwave plasma to beat thermodynamics in CO_2 dissociation," *Faraday discussions*, vol. 183, pp. 233–248, 2015.

[74] N. den Harder, D. C. M. van den Bekerom, R. S. Al, M. F. Graswinckel, J. M. Palomares, F. J. J. Peeters, S. Ponduri, T. Minea, W. A. Bongers, M. C. M. van de Sanden, and G. J. van Rooij, "Homogeneous CO_2 conversion by microwave plasma: Wave propagation and diagnostics," *Plasma Process. Polym.*, vol. 14, p. e1600120, 2017.

[75] A. Boagerts and E. C. Neyts, "Plasma technology: An emerging technologyfor energy storage," *ACS Energy Lett.*, vol. 3, pp. 1013–1027, 2018.

[76] J. F. de la Fuente, A. A. Kiss, M. T. Radoiu, and G. D. Stefanidis, "Microwave plasma emerging technologies for chemical processes," *J. Chem. Technol. Biotechnol.*, vol. 92, pp. 2495–2505, 2017.

[77] G. Raposo, "Plasma in-situ production of fuel and oxygen on Mars," Master's thesis, Instituto Superior Técnico, Universidade de Lisboa, Portugal, 2020.